High-Resolution Transmission Electron Microscopy Studies of Sol–Gel-Derived Cobalt-Substituted Barium Ferrite

Geok B. Teh[1] and David A. Jefferson

Department of Chemistry, University of Cambridge, Lensfield Road, Cambridge CB2 1EW, United Kingdom

Nanocrystal specimen of cobalt (II)-doped magnetoplumbite (*M*-type) $BaFe_{12}O_{19}$ were synthesized via a sol–gel method using ethylene glycol as precursor. Hexagonal-like platelets and other morphologies of ferrites were obtained at the final stage of annealing process. The specimens were characterized using X-ray diffraction, SQUID magnetometry measurement and high-resolution transmission electron microscopy. The saturation magnetization of the specimen at 300 K was found to be greatly reduced from 48 (3) emu/g in parent ferrite to 28 (3) emu/g in the doped ferrite. A total reduction of 74% in the value of intrinsic coercivity was recorded, 276 (15) G from the doped ferrite compared to 1080 (54) G in the parent ferrite. © 2002 Elsevier Science (USA)

Key Words: barium ferrite; sol–gel; hysteresis; high-resolution electron microscope; spinel; iron oxide; nanocrystal; coercivity; cobalt substitution; hexagonal ferrite.

1. INTRODUCTION

Over the past few decades, the sol–gel method has been used extensively to produce fine particles of a variety of oxides (1–4). With the increasing demands for an erasable high bit density data storage system, fine particle of cation-substituted barium ferrite are widely anticipated to be a suitable candidate for future high-density magneto-optical recording (5). It is known that magneto-optical effects in the magnetic recording may be substantially enhanced by ion substitution (6).

The parent ferrite, $BaFe_{12}O_{19}$ is a hexagonal hard ferrite which has space group of $P6_3/mmc$ (7). Because of its high interest as a material suitable for perpendicular magnetic recording, many efforts have been devoted to the produc-

tion of suitable cation-substituted barium ferrite which is of finer particles (8, 9).

In barium ferrite, cobalt substitution has been the subject of many reports (8–10), but so far, none has been fully characterized using high-resolution transmission electron microscopy. This paper focuses on the high-resolution work on the crystals of cobalt-substituted barium ferrite. The sol–gel method route was employed in this work in an attempt to achieve higher homogeneity in the final product.

2. EXPERIMENTAL

The synthesis of $BaCo_XFe_{12-X}O_{19}$ ($x = 1.0$) was performed using the sol–gel route. Ethylene glycol was used as precursor where stoichiometric weight of $Ba(NO_3)_2$, $Co(NO_3)_2 \cdot 6H_2O$ and $Fe(NO_3)_3 \cdot 9H_2O$ was dissolved at a temperature of 50°C for 2 h. The homogeneous solution was then placed under an IR lamp for dehydration to occur which enhanced the gelation process. The dried gel which contained the finely mixed oxides of the starting materials was then annealed at a temperature of 800°C($\pm$20°) for 3 days with intermediate grindings and was quenched in the air.

X-ray diffraction patterns were recorded at the Philips Diffractometer type PW1710. The Philips system is composed of a vertical goniometer without a monochromator, controlled by the Philips PC-APD software. The X-ray tube with a copper target ($K\alpha = 1.54060$ Å) was operated at 40 kV and 40 mA. About 20%wt of hand-milled silicon powder was mixed into the sample as the internal standard. The samples were smeared onto a microscope slide with a droplet of iso-propanol. Routine step scanning was then carried out from 5.0° to 80.0° ($2\theta°$) with a step size scan of 0.020°/1.5 s ($2\theta°$).

Chemical composition analysis was carried out by energy dispersive X-ray spectroscopy (EDS) on a JEOL EM-2010 electron microscope. The magnetic properties of

---

[1] To whom correspondence should be addressed. Kolej Tunku Abdul Rahman, Kampus Jalan Genting Kelang, Peti Surat 10979, 50932 Kuala Lumpur, Malaysia. Fax: +603-40226336. E-mail: tehgb@mail.tarc.edu.my.

the samples were measured with the superconducting quantum interference device (SQUID) at the Interdisciplinary Research Centre in Superconductivity (IRC), University of Cambridge. The hysteresis loops were recorded between $-13.5 \, \text{kG} \leq H \leq 13.5 \, \text{kG}$ at 300 K.

The HRTEM micrograph of the sample was obtained from JEOL 200CX electron microscope at a magnification of 190,000–300,000 ×, after carefully correcting the objective lens astigmatism and incident beam inclination using the granularity of the carbon support film.

3. RESULTS AND DISCUSSIONS

A nominal doping rate of 1.0 is chosen as the M-type structure remains ferromagnetic (9) along the $0 \ll X \ll 2.0$. As the substitution was about 8.3% of the molar ratio of ion Fe^{3+} in the parent ferrite, we can be sure that whatever drastic magnetic changes that occurred is due to the cobalt substitution and not because of the great loss of Fe^{3+} in the process of ion substitution.

3.1. X-Ray Powder Diffraction

Figure 1 shows the X-ray diffraction patterns of the parent ferrite $BaFe_{12}O_{19}$ and the cobalt-substituted $BaFe_{12}O_{19}$. Lattice constants were calculated from (110),

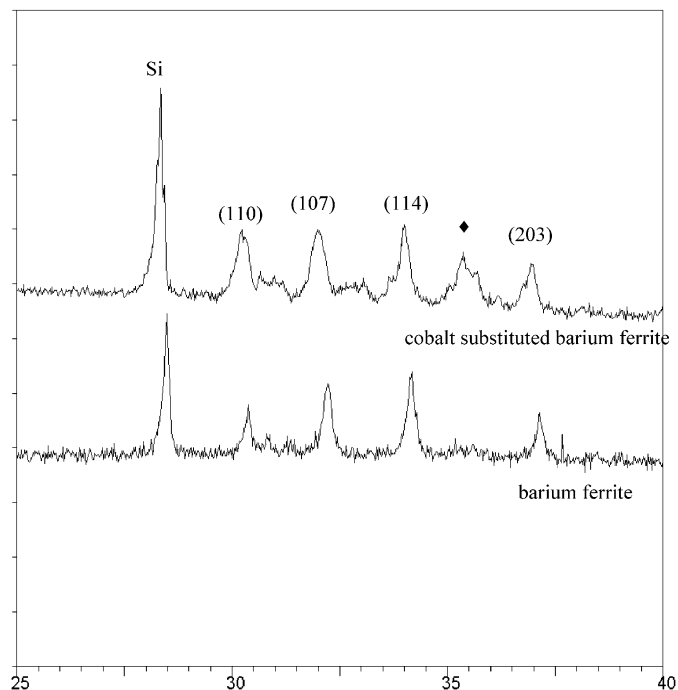**FIG. 1.** Region of XRD pattern for the parent ferrite, $BaFe_{12}O_{19}$ and cobalt-substituted barium ferrite, $Ba_{1.0}Co_{1.3(1)}Fe_{11.6(3)}O_{19}$. Peak marked as 'Si' is the peak for the silicon powder which was added as internal standard. Peak marked '♦' is the (200) reflection from Fe_2O_3, iron oxide.

TABLE 1
XRD Results Shows the Lattice Parameters and Cell Volumes in $BaMFe_{11}O_{19}$ with the Substitution of Ion Co^{2+} Compared to the Parent Ferrite

Ion M	a (Å)	c (Å)	V (Å)
Fe^{3+}	5.8891 (5)	23.192 (5)	696.6 (1)
Co^{2+}	5.886 (2)	23.23 (2)	696.8 (6)

(107), (114) and (203) reflections. All the reflections were indexed on the basis of the magnetoplumbite structure, keeping the $P6_3/mmc$ space group (7). A (200) reflection from Fe_2O_3 is detected in the cobalt-substituted barium ferrite. At one stage, this peak was thought to be from the unreacted iron oxide particles. However, in the HRTEM work, a crystal that consists of two phases both of barium ferrite and iron oxide was found (see Fig. 3). The morphology of that crystal will be discussed in the later section. The finding of such crystal thus explained the (200) reflection in the XRD pattern. The changes in cell volumes when ion Fe^{3+} was being substituted in the parent ferrite is relatively not significant as shown in Table 1. The unit cell for cobalt-substituted barium ferrite contracts in a-axis and expands in c-axis, resulting in a small increase in a cell volume of 0.03%. However, the results are not significant to be discussed further. The X-ray diffraction method applied in this study cannot provide the required information about the cation substitution due to the similar scattering power of all the ions involved.

3.2. EDS and Particle Size Determination

The average particle size of the samples in our study were deduced from the width of XRD maxima by applying the classical Scherrer equation (11,12). The broadening of the selected peaks and the silicon peaks which acted as the internal standard were measured and replaced in the Scherrer equation which thus gives the average particle size of the specimen. From Table 2 it shows that the cobalt-substituted barium ferrite is slightly smaller in size compared to the parent ferrite, varied about 100 Å. The variation in sizes of the both ferrites was not significantly

TABLE 2
EDS and Particle Size Results for Barium Ferrite and Cobalt-Substituted Barium Ferrite

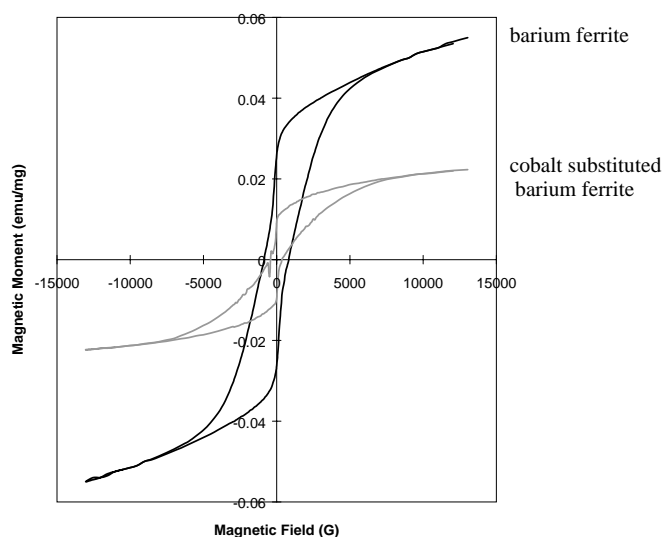| Ferrites	Calculated particle size using the Scherrer equation (Å)	EDS composition
$BaFe_{12}O_{19}$	360 (20)	$Ba_{1.0}Fe_{11.8(9)}$
$BaFe_{11}CoO_{19}$	260 (15)	$Ba_{1.0}Fe_{11.6(3)}Co_{1.3(1)}$

FIG. 2. Hysteresis loops of barium ferrite and cobalt-substituted barium ferrite.

great in our study. However, as nanoparticles are known to exhibit different surface properties and magnetic properties compared to bulk particles, this size variation observed is nevertheless expected to influence the magnetic properties of the final cobalt-substituted ferrite.

3.3. SQUID Magnetometry Measurements

Figure 2 shows the hysteresis loops of both the parent ferrite and the cobalt-substituted barium ferrite. It is clearly evident that cobalt substitution in $BaFe_{12}O_{19}$, reduced the intrinsic coercivity from 1080 (54) G in parent ferrite, $BaFe_{12}O_{19}$, to 276 (15) G. The substitution of cobalt also reduced the saturation magnetization by 20 emu/g. The remanent magnetization of the parent ferrite, $BaFe_{12}O_{19}$, was recorded as 25 (2) emu/g and the cobalt-substituted ferrite was as 15 (2) emu/g. It is obvious that cobalt-substitution reduced $BaFe_{12}O_{19}$ to a softer ferrite. The area of hysteresis loss per cycle in the cobalt-substituted barium ferrite is relatively smaller compared to the parent ferrite, which is a very good characteristic for recording media.

3.4. HRTEM Imaging

Figure 3 shows a crystal of cobalt-substituted barium ferrite which is characterized by a central region with a lattice fringe spacing of 2.77 Å. At the outer edge of the particle, the arrangement of lattice fringes is similar to the parent ferrite, $BaFe_{12}O_{19}$. There are two orientations of the ferrite component present, with an angle of approximately $70°$ between them, measured from the power spectrum of the image which is shown as an insert in Fig. 3. This corresponds to the angle between the close-packed planes

in a spinel structure when viewed down [110]. The crystal therefore consists of a center with a cubic close-packed array of oxygen and iron ions which is then encapsulated by a ferrite phase. The cubic close-packed nature of the center of the crystal in Fig. 3 suggests that it is the spinel Fe_3O_4, but the possibility that all the Fe is present in the trivalent state cannot be ruled out and the γ-Fe_2O_3 defect spinel structure would look the same. The presence of crystallites of this type could well explain the high Fe peak intensity in the EDS analysis. The crystal could be regarded as an intermediate product in the formation of a hexagonal platelet of cobalt-substituted barium ferrite. With the assumption of the center of the crystal being a spinel-structured Fe_3O_4, the misfit of metal–metal distances in the (001) plane of barium ferrite and the (111) plane of spinel Fe_3O_4 is 0.97%. This is due to the metal–metal distance of (001) plane in $BaFe_{12}O_{19}$ being 5.88 Å and metal–metal distance in the (111) plane of spinel Fe_3O_4 being 5.937 Å. However, this misfit does not show any strain in the grain boundaries observed.

4. CONCLUSIONS

The results presented in this paper indicate that cobalt substitution in barium ferrite using sol–gel method can significantly decrease the intrinsic coercivity and saturation magnetization of the barium ferrite, $BaFe_{12}O_{19}$. The particle size of samples obtained through the suggested
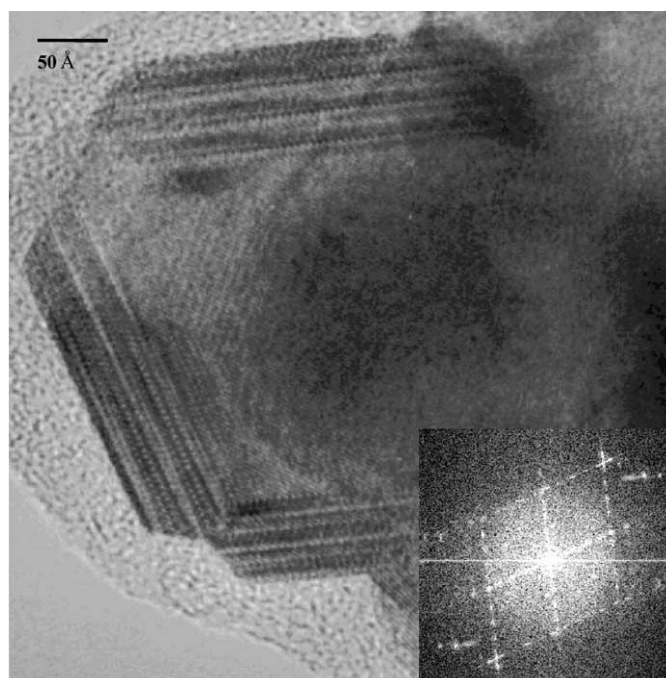

FIG. 3. HRTEM micrograph of a spinel crystal encapsulated by M-type ferrite in the specimen of cobalt-substituted barium ferrite, $Ba_{1.0}Co_{1.3(1)}Fe_{11.6(3)}O_{19}$.

synthetic route confirmed to be of nanosized. The phase of barium ferrite is proven to be crystallized on the {111} planes of spinel-structured iron oxide. High-resolution electron microscopy proved to be a good method to detect crystals of interest and provided helpful information on the crystal structure and the crystal defects that existed in the final samples.

ACKNOWLEDGMENTS

REFERENCES

1. G. De, L. Tapfer, M. Catalano, G. Battaglin, F. Caccavale, F. Gonella, P. Mazzoldi, and R. F. Haglund Jr., *Appl. Phys. Lett.* **68**(26), 3820–3822 (1996).

2. C. Surig, K. A. Hempel, and D. Bonnenberg, *Appl. Phys. Lett.* **63**(20), 2836–2838 (1993).

3. C. Surig, K. A. Hempel, and D. Bonnenberg, *IEEE Trans. Magn.* **30**(6), 4092–4094 (1994).

4. X. Wang, D. Li, and L. Lu, *J. Alloys Compd.* **237,** 45–48 (1996).

5. H. Nakamura, F. Ohmi, Y. Kaneko, Y. Sawada, A. Watada, and H. Machida, *J. Appl. Phys.* **61**(8), 3346–3348 (1987).

6. A. Grusková, *IEEE Trans. Magn.* **30**(2), 639–641 (1994).

7. J. Smit and H. P. J. Wijn, "Ferrites: Physical Properties of Ferromagnetic Oxides in Relation to their Technical Applications," Philips Technical Library, 1959.

8. R. Carey, P. A. Gago-Sandoval, D. M. Newman, and B. W. J. Thomas, *J. Appl. Phys.* **75**(10), 6789–6791 (1994).

9. X. Battle, X. Obradors, J. Rodríguez-Carvajal, M. Pernet, M. V. Cabañas, and M. Vallet, *J. Appl. Phys.* **70**(3), 1614–1623 (1991).

10. X. Battle, M. García del Muro, J. Tejada, H. Pfeiffer, P. Görnert, and E. Sinn, *J. Appl. Phys.* **74**(5), 3333–3340 (1993).

11. M. H. Loretto, "Electron Beam Analysis of Materials," Chapman & Hall, New York, 1984.

12. A. Wold and K. Dwight, "Solid State Chemistry: Synthesis, Structure & Properties of Selected Oxides & Sulfides," Chapman & Hall, New York, 1993.